Analyst

PAPER

View Article Online
View Journal | View Issue

Cite this: *Analyst*, 2014, **139**, 6249

Impact of pulse duration on localized single-cell nano-electroporation†

Tuhin Subhra Santra,[a] Hwan-You Chang,[bc] Pen-Cheng Wang[d] and Fan-Gang Tseng*[ade]

Received 9th June 2014
Accepted 20th September 2014

DOI: 10.1039/c4an01050g

www.rsc.org/analyst

We introduce a localized single-cell membrane nano-electroporation with controllable sequential molecular delivery by millisecond to nanosecond electrical pulses. An intense electrical field was generated by a pair of transparent indium tin oxide (ITO)-based nano-electrodes, which was confined to a narrow region of the single-cell membrane surface near the nano-electrode edges (approximately 2 μm × 50 nm area), whereas the remaining area of the membrane was unaffected. Moreover, a 250 nm SiO_2 passivation layer on top of the nano-electrode reduced not only the thermal effect on the cell membrane surface, but it also avoided the generation of ions during the experiment, resulting in the reduction of cell toxicity and a significant enhancement of cell viability. Our approach precisely delivers dyes, Quantum Dots (QDs) and plasmids, through a localized region of single HeLa cells by considerably enhanced electrophoresis and diffusion effects with different duration of the pulsing process. The smaller molecules took less time to deliver into a single cell with a single pulse, whereas larger biomolecules took longer time even for multiple numbers of long lasting pulses. The system not only generates sequential well-controlled nano-pores allowing for the rapid recovery of cell membranes, but it also provides spatial, temporal and qualitative dosage control to deliver biomolecules into localized single-cell levels, which can be potentially beneficial for single cell studies and therapeutic applications.

1. Introduction

The introduction of foreign biomolecules into targeted living cells is an important phenomenon for biological and therapeutic applications. Many of the transfection techniques have been developed, including viral vectors,[1,2] chemical methods (such as basic protein and complexes with lipids, as well as calcium phosphate[3]) and physical methods (including particle bombardment, micro-injection,[4] jet injection,[5] sonoporation,[6] lipid-mediated entry into cells[7] and electroporation).[8–11] Viral vectors have certain limitations for gene transfer, such as immune response, toxicity, and high cost.[12,13] However, physical methods are potentially substitute tools for gene transfer without these limitations.[14] Among all the physical methods, electroporation techniques have the advantages of easy operation, rapidity, greater reproducibility due to the determination of electrical parameters, avoidance of toxicity and easy controlling of the size of electropores with reduced leakage of the cytosolic component.[15] However, this process has pH variation, electrical-field distortion and thermal effect due to large surface electrodes, exhibiting low cell viability.[16–18] The molecular transportation inside and outside of the cell during electropermeabilization is relatively nonspecific and causes the ionic imbalance, leading to improper cell function and finally cell death.[19] With regards to single-cell electroporation (SCE), because of the application of a high external electrical field, the conductivity of the cell cytoplasm and extracellular medium can increase by several orders of magnitude compared to cell membrane. The intracellular and extracellular conductivities become different, as a result, the cell membrane can act as a capacitor, which can store electrical charges onto the membrane by the function of ion channels and ion pumps.[20] This difference is known as transmembrane potential (TMP), which can be expressed by Schwan's equation as follows:

$$\mathrm{TMP} = \varphi_i - \varphi_e = 1.5 r E_0 \cos\theta,$$

where $\varphi_i - \varphi_e$ is the potential difference between intracellular and extracellular membrane, r is the radius of the cell, E_0 is the strength of the applied electrical field and θ is the angle between

[a]*Institute of Nano Engineering and Microsystems, National Tsing Hua University, Taiwan. E-mail: santra.tuhin@gmail.com*

[b]*Institute of Molecular Medicine, National Tsing Hua University, Taiwan. E-mail: hychang@life.nthu.edu.tw*

[c]*Department of Medical Science, National Tsing Hua University, Taiwan*

[d]*Department of Engineering and System Science, National Tsing Hua University, Taiwan. E-mail: wangpc@ess.nthu.edu.tw*

[e]*Division of Mechanics, Research Centre for Applied Sciences, Academia Sinica, Taiwan. E-mail: fangang@ess.nthu.edu.tw; Tel: +886-3-571-5131 ext. 34270*

† Electronic supplementary information (ESI) available. See DOI: 10.1039/c4an01050g

the direction of electrical field and selected point of the cell surface.[21,22]

Recently, several groups developed MEMS-based devices for single-cell electroporation studies. The miniaturization of the gap between two electrodes resulted in an intense electric field at the gap region, which can easily turn the adjacent impermeable membrane into a permeable one to transport the foreign bio-molecules inside the cell with high transfection rate and high cell viability to reduce electrode surface area, which lead to faster heat dissipation into the microfabricated chip.[23,24] SCE has been demonstrated by patch clamp,[25,26] atomic force microscopy (AFM) techniques[27] and microfluidic devices.[28–31] Recently, some techniques demonstrated localized single-cell electroporation with complex fabrication and higher voltage requirements.[9,27,32–34] To intensify an electric field in a very specific region of a single cell, AFM is one of the most promising techniques. However, AFM technique cannot be easily extended into in-parallel position. In our earlier work, we have shown molecular dye delivery with constant pulse duration and various applied voltages, where to increase voltages, the affected membrane area also increased and finally lead to cell death.[35] In the present work, we demonstrate the effect of different durations of pulses with fixed external applied voltage. The different duration of pulses can form different sizes of nanopores into a specific membrane area to deliver biomolecules with high cell viability. We have fabricated a very simple and low-cost microfluidic device for localized single-cell nano-electroporation (LSCNEP), which is based on multiple numbers of nano-electrode arrays formed by focused ion beam (FIB) technique. The nano-electrodes were fabricated with a thickness of 90 nm, gap of 500 nm and depth of 3 μm between two ITO nano-strips, which can intensify an electrical field in-between the nano-electrode gap. As a result, localized single cell membrane nano-electroporation can be performed with high transfection rate and high cell viability. Due to the very small electrode surface area and small electrode gap, the field distortion and temperature effect should be reduced on the cell membrane, providing an increase in cell viability. Moreover, in our device, a 250 nm SiO_2 layer was deposited on the top of the ITO nano-electrode, which not only avoids high electrical shock on the cell membrane surface, but it also reduces thermal effect with the generation of hydroxyls and hydrogen ions, causing high toxicity in between the two nano-electrode surfaces. Our system successfully delivers very fast QDs/plasmids inside the single cell with higher pulse durations and lower voltage requirement. This LSCNEP device can easily control sequential molecular delivery through a specific region of the single cell with adjustable pulse duration and number of pulses. As a result, it might control ionic balance between outside and inside of the cell membrane to avoid improper cell function and cell death during the electroporation process.[16–18]

2. Experimental section

2.1 Design and simulation

As shown in Fig. 1 and Fig. S1, (ESI† material, only the red part is highlighted for simulation results), the schematic representation of the localize single-cell nano-electroporation (LSCNEP) overlap with electrical field simulation results, in which two nano-electrodes are set 500 nm apart, and a single HeLa cell is seeded as semi-hemisphere (see Fig. 1) on the top of the nano-electrode. As anticipated by simulation results (Comsol Multiphysics 3.5 version, Sweden), the electrical field is more intensively generated on the localized membrane region of the single cell. Fig. 1(a) shows the electrical field distribution on the localized HeLa cell membrane surfaces. Fig. 1(b) shows a resistive heat effect on the cell membrane, where the maximum heat generation is formed on the edge of the ITO nano-electrodes, which cannot affect the cell membrane due to 250 nm SiO_2 passivation layer on the top of the nano-electrode. Fig. 1(c) shows the electrical field distribution on SiO_2 and cell membrane interface. Due to the SiO_2 layer, the electrical field effect is avoided on the cell membrane surface area (those areas are attached with the electrode surface, but not in the gap region), except for the nano-electrode gap region. The electrical field intensity was considerably higher on the edge of the two nano-electrodes surface (1.8×10^8 V m^{-1}), and it continuously reduces towards the center of the gap (at $x = 0$). Fig. 1(d) shows the effect of the resistive heat (3.1×10^{10} W m^{-3}) on the cell membrane, where heating affected only the edge of two nano-electrodes. If we consider our LSCNEP chip without SiO_2 layer, then electric field (6×10^8 V m^{-1}, see ESI material Fig. S2†) and resistive heat (0.35×10^{12} W m^{-3}, see ESI material Fig. S3(a)†) not only affect the nano-electrode gap region, but it also affects the larger area of cell membrane surface (those membrane area is attach with electrode surface area). This similar phenomena was experimentally observed, where external voltage was applied (4 Vpp, 5 ms pulse) in specific two electrodes with HeLa cells (see ESI Fig. S4(a)†) and immediately LSCNEP chip was incubated for an hour. Subsequently, PI (propidium iodide) dye was delivered into the chip, and it stained the nucleus of dead cells, resulting in red fluorescence imaging (see ESI Fig. S4(b)†). This dead-cell imaging appears only from two electrode surface where we had applied voltages. None of the other electrode surface was affected (we did not apply the voltage to the other electrodes, see ESI Fig. S4(b)†). From simulation results without a SiO_2 layer, the electrical field and resistive heat is much higher (for 6 Vpp) when compared to that with SiO_2 layer (see Fig. 1 and ESI S2 and S3†). As a result from our experiment without the SiO_2 layer, we sometimes observe bubble generation at lower voltages (3–5 Vpp) and single cell bursts at higher voltages (over 5 Vpp) with very low cell viability (<30%) (see ESI Fig. S5†). Therefore, we employ SiO_2 layer passivation to prevent bubbles, as well as hydrogen and hydroxyl ion generation at higher voltages (6 Vpp). Fig. 1(e) shows *trans*-membrane potential (TMP) values for an externally applied voltage (6 Vpp) with the consideration of SiO_2 layer. The TMP value approaches the maximum (0.8 V) at the edge of the nano-electrode (50 nm approximately) and continuously reduces towards the middle of the nano-electrode gap. However, without the consideration of SiO_2 layer, the TMP value is approximately 3 V (ESI material Fig. S3(b)†), which spreads all over the cell membrane surface attached with the nano-electrode surface area, and the value sharply decreases (almost zero) at the center of the nano-

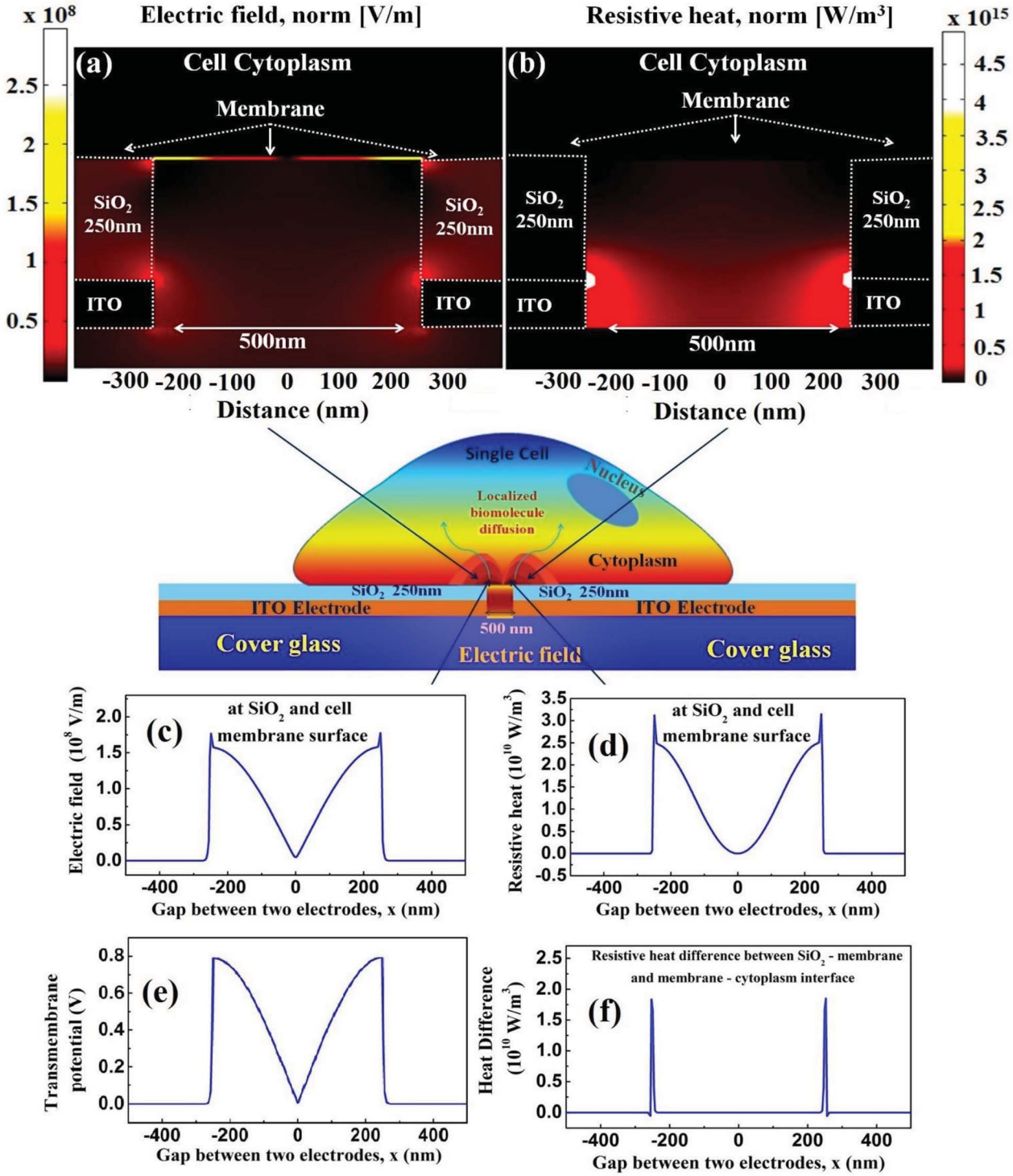

Fig. 1 Electrical field and resistive heat simulation results on HeLa cell for localized single-cell membrane nano-electroporation: (a) electrical field distribution on the HeLa cell membrane; (b) resistive heat distribution; (c) electric field distribution between the SiO_2 layer and cell membrane interface; (d) resistive heat effect at the SiO_2 and cell membrane interface; (e) transmembrane potential distribution (TMP) on the cell membrane surface; and (f) resistive heat difference between SiO_2-membrane and membrane cytoplasm interface.

electrode gap. This TMP value significantly exceeded compared to the cell membrane threshold values (0.2–1 V) easily resulting in cell death. Fig. 1(f) shows the resistive heat difference between SiO_2-membrane and membrane cytoplasm interface (the heat difference is 1.8×10^{10} W m^{-3} at the edge of two nano-electrodes). The maximum electrical field and resistive heat act together to affect only the small areas of the cell membrane (approximately 2 μm × 50 nm area for 0.6–0.8 V TMP values) on

the edges of each nano-electrode. It is suggested that the maximum amount of membrane nano-pores with larger sizes are formed on the edge of the two nano-electrodes, and the sizes are continuously reduced toward the center ($x = 0$), where the strength of electrical field, heat generation and TMP values are almost zero.

2.2 Fabrication

Fig. 2(a) shows the fabrication process step of the nano-electroporation chip. Initially, a cover glass slide (24 mm × 30 mm, Deckglaser, Germany) was cleaned by piranha solution with 7 : 1 ratio of sulphuric acid (H_2SO_4) and hydrogen peroxide (H_2O_2) at 80 °C for 10 min. 90 nm of ITO film was then deposited by RF sputtering on the top of the cover glass slide and the film was immediately annealed at 330 °C for 3 h to increase the film uniformity and conductivity. The resistivity of deposited ITO film was 5.4×10^4 ohm cm^{-1}, which was measured by the four point probe method (Napson Corporation, Japan). The light transparency of the deposited ITO film was 85–98% with a visible-light range from 450 nm to 800 nm, which was measured by UV-VIS (Jasco, V-670 spectrometer, USA) spectroscopy (see Fig. S6(a), ESI† material). The X-ray diffraction (XRD) results show that the films have proper orientation[36] (see Fig. S6(b), ESI† material). After ITO deposition, the film was patterned by wet chemical etching with 1 : 3 ratios of hydrochloric acid (HCl) and water (H_2O) solution at 40–50 °C for 3–4 min. Fig. 2(b) shows the scanning electron microscopy (SEM) image of the ITO lines. The patterned ITO lines were etched by focused ion beam (FIB) technique with a 500 nm gap and 3 μm depth to form a ITO nano-electrode with a microfluidic channel (see Fig. S7, ESI† material). Fig. 2(c) shows the ITO nano-electrodes with a 500 nm gap between two nano-electrodes. After the formation of the nano-electrodes, 250 nm SiO_2 layer was deposited on the top of the nano-electrodes surface by plasma enhanced chemical vapor deposition (PECVD) technique. The final device was packaged with printed circuit board (PCB), which is shown in Fig. 2(d).

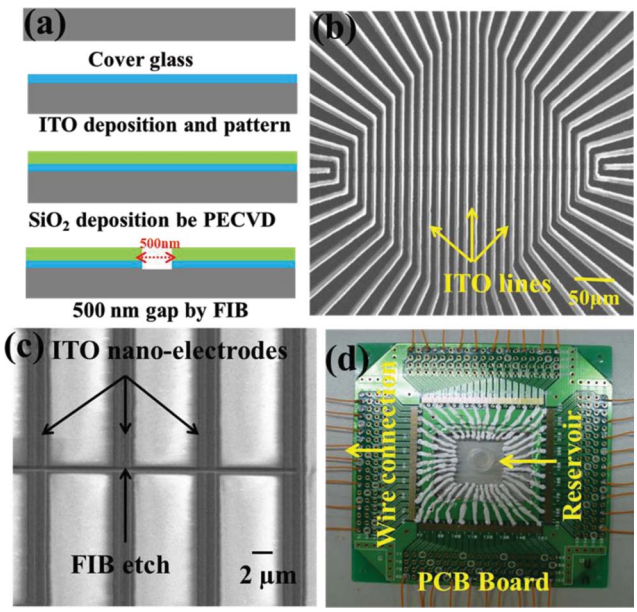

Fig. 2 Fabrication process of a nano-electrode-based transparent chip: (a) fabrication process step; (b) SEM image after wet chemical etch of ITO lines; (c) FIB etched ITO nano-electrode (electrode width = 2 μm, electrode gap = 500 nm and electrode thickness = 90 nm, the depth of the gap from electrode surface = 3 μm to make as microfluidic channel); (d) final packaging of fabricated ITO nano-electrode-based transparent chip.

2.3 Cell preparation

For the LSCNEP experiment, we used HeLa (human cervical cancer) cells, which is an immortal cell line for scientific research. To culture HeLa cell lines, old medium was initially removed from the cell culture dish and 10 ml of phosphate buffer saline (PBS) was added to properly clean the cell surface. The cleaning process was performed two to three times. Subsequently, 1 ml trypsin (0.05% trypsin-EDTA, GIBCO) was added into the cell culture dish and incubated for 5–7 min to detach the cells from the dish surface. 9 ml DMEM (Dulbecco's modified Eagle's Medium containing 1% sodium pyruvate, 1% non-essential amino acids and 1% penicillin streptomycin) medium was then added and properly mixed with the cells. The cells were suspended with DMEM medium, and they were ready to be transferred into the LSCNEP chip container.

2.4 Chip surface modification for the enhancement of the cell adhesion

To improve cell adhesion on the chip surface, collagen (Sigma, St Louis, MO, USA) was added into the chip container with a concentration of 10 μl ml^{-1}. UV light illumination was then introduced for 2 h for sterilization. Finally, the chip was cleaned with ddH_2O to release all unbound collagen residue from the chip surface. After washing, DMEM medium with the cells was added into the chip container at a concentration of 2.2×10^5 cells per ml and the cell with chip was incubated (5% CO_2, 37 °C) for 16–20 h to adhere cells into the chip surface. When the cells were strongly attached on the surface of the nano-electrodes, the chip was ready for experimentation.

2.5 Fluorescence microscopy

For the LSCNEP process, inverted fluorescence microscopy (Olympus IX71, Melville, NY) was used with 20× objective lens (numerical aperture (NA) = 0.40). The fluorescence excitation was provided using a 100 W mercury lamp with a bright field configuration. The excitation and emission of the PI dye and QD (deep-red COOH group) were Ex.510-550BP/570DM/Em.590LP and Ex.545-580BP/600DM/Em.610LP. However, for plasmids (pMax E_2F_1), the excitation and emission were 475–495 nm and 520–560 nm, respectively. To visualize the cell-surface layers, Z scan was performed with confocal microscopy after QD was delivered into the HeLa cells. The step size was 1 μm. The exposure time and gain was fixed at 5000 ms and 20 dB. The QD scanning image was observed by a 532 nm argon laser source.

2.6 Image analysis

Images were initially recorded (for PI dye and Quantum Dot tracking) by a fluorescence microscope with different time scales. Image-Pro Plus software (Media Cybernetics, USA) was used to analyse the intensity using line profile function to draw the line from the centre of the cell. Finally, this line profile data were fitted by ORIGIN software (Massachusetts, USA) to calculate intensity variation (arbitrary unit) with time.

2.7 Localized electroporation procedure

After 16–20 h incubation of HeLa cell onto the LSCNEP chip, concentration 2.2×10^5 cells per ml, the cells were strongly attached and randomly distributed throughout the chip surface. External voltages were applied only to those single cells attached on the top of the nano-electrodes surface. Before voltage and pulse applications, the cell surfaces were washed with PBS. 200 μl PBS was then introduced with a sufficient amount of dye/QDs/plasmid, and immediately the required pulses and voltages were applied. Various voltages (1–8 Vpp) and single square wave positive pulses (15 ms, 500 μs, 50–200 ns) were applied into the LSCNEP chip by a function generator (WW5061, Tabor Electronics, Israel). However, to study the effect of pulse duration for nano-electroporation, a voltage of 6 Vpp was applied in each case for better delivery rates with higher cell viability. Due to sufficient voltage and pulse application, cell membranes deformed and created transiently permeable nano-pores to allow dyes/biomolecules from the outside to the inside of the single cell. The most possible diffusion occurred at the nano-pore region, which was distributed along the two nano-electrodes gap connected with microfluidic channel (see Fig. 2(c) and S7 in ESI† material). Fig. S8 (see ESI† material for example) shows randomly distributed HeLa cells throughout the chip surface, and we selected to apply voltage on three single cells located in between the two nano-electrodes. External voltage can be applied either separately into individual cells or simultaneously into all cells for effective comparison. In the current experiment, voltage and pulse were applied separately into each single HeLa cell.

2.8 Delivery rate and viability test

To calculate the delivery rate and cell viability for different pulse durations, each experiment was performed more than 10 times and the data was averaged to obtain the final values. The delivery rate was calculated by each single-cell response with molecular dye after an external applied voltage on the cell. The cell viability was tested using cell-permeable calcein AM (for live cells) solution and cell-permeable propidium iodide (PI) (for dead cells) dye. The permeable calcein AM can perform hydrolysis inside the live cell and produce green colour cytoplasm for viable cells, while colour will be absent for dead cells. The PI dye can interact with the nucleus of the dead cell to produce a red fluorescence image, while for live cells, the colour will be absent due to the lack of interaction inside the cell.

3. Results and discussion

3.1 Nano-electrode design for LSCNEP process

To achieve an excellent electroporation, voltage, pulse duration and the number of pulses need to be properly controlled, which depends on the following requirements: first, the threshold membrane potential must be achieved to create membrane nanopores. Second, stable nano-pores must be formed; membrane nano-pores should be converted from hydrophobic to hydrophilic, which depends on pulse duration and the number of pulses. Finally, the cell membrane should be resealed without any mechanical rupture or any type of injury on the cell membrane, which depends on the externally applied voltage and heat generated during the electroporation process.[37–40] Biomolecules can be transported only at the last two stages, where the membrane opening to resealing is in a complete phase. In our design, we reduce the electrode gap size down to 500 nm, and the resulting electrical field was significantly concentrated at the edge of the gap region, leading to a reduction in the applied voltages for overcoming the cell membrane threshold voltages.

3.2 Role of SiO_2 passivation layer

A 250 nm SiO_2 layer was deposited for the passivation of the electrical field. The width of each nano-electrode was 2 μm with a thickness of 90 nm. As a result, each nano-electrode area was small, and it can generally provide higher electrical resistance, which causes a low current.[18] This low current induced a lesser chemical reaction in between two nano-electrode gap. Due to the application of a very strong external electrical field, the formation of bubbles and turbulent flow should be considered, in addition to the Joule heating limitation. Fig. S5 (ESI† material) shows bubble generation during the electroporation experiment (3–6 V was applied) without SiO_2 layer on the chip. As a result, cell viability was very low (<30%). To avoid these effects, the electrical field was passivated by the SiO_2 layer, which can effectively reduce the gas evolution and Joule heating effect on the cell membrane surface while still allowing sufficient electrical fields for nano-pores generation.

3.3 Electric pulse effect

3.3.1 Millisecond, microsecond and nanosecond pulse effects. The sequential LSCNEP processes were successfully observed with different voltages and different pulse durations. Among different applied voltages, 6 Vpp (peak to peak) single square wave positive pulse was optimized to provide a better delivery rate with high cell viability. The sequential transfection is important due to the requirement of knock-down pre-expressed signals or periodic transfection.[32,41–44] However, it is difficult to achieve high efficiency by this transfection.[45] When the single cell was positioned (randomly) in between the top of the two nano-electrodes, voltages and pulses were sequentially applied to the selective electrode pair in the presence of PI dye surrounding the cell. Due to the application of sufficient voltage (6 Vpp, 15 ms pulse), the transmembrane potential exceeds the cell

membrane threshold values, and it creates transiently permeable nano-pores on the cell membrane. Immediately, the PI dye entered into the single cell (through microfluidic channels connected to a nano-electrode gap) by diffusion due to a high-concentration gradient surrounding the membrane nano-pores, resulting in a red fluorescent image. Fig. 3(a)–(c) shows the fluorescent images of HeLa cells that survived for 6 Vpp 15 ms, 500 μs and 100 ns pulses, where the continuously intensity increases with increase in time, and after a certain time, intensity was saturated. Fig. 4(a) shows intensity distribution profiles for 15 ms pulse with a cell membrane self-recovery process. The pulses were applied at each 100 s duration. The results show that after the application of the first pulse, intensity sharply increases and then saturates, which indicates long-lived nano-pores were initially opened up on the cell membrane, and after sometime the membrane tries to reseal the nano-pores again (approximately 40–50 s, and then turns into saturation mode). After the applications of second (at 100 s) and third pulses (at 200 s), the nano-pores were re-opened again and the dye could enter inside the cell. As a result, the intensity sequentially increased during each pulse and then accordingly saturated. After the application of fourth pulse (at 300 s), the intensity was almost constant without further increment, indicating that the concentration of PI dye inside and outside the cell became similar, or the concentration gradient across the nano-pores became zero. As a result, PI dye stopped to enter inside the cell whether the nano-pores opened or not. Fig. 4(c), shows the fluorescence intensity distribution of single cell stimulated by 6 Vpp 500 μs pulses. In this condition, intensity saturation took a longer time (800 s), which indicated that under either a microsecond or millisecond pulse, the density of the generated nano-pores were the same because of the same applied voltage (6 Vpp) on the same area of the membrane, but the average opening area of the nano-pores were smaller for microsecond pulse duration. It has been reported that affected membrane area can depend on the applied voltage and amplitude of the pulse.[35,46] However, the affected nano-pores area can depend on pulse duration and number of pulses.[47,48] For nanosecond pulse, the applied voltage was 6 Vpp with 100 ns. From Fig. 4(e), the fluorescence intensity initially increased very slowly (pulse applied at 0 s). It might be that a single ultra-short pulse cannot open the sufficient number of nano-pores (*i.e.* hydrophilic pores) with larger sizes in the first electric pulse. When the second pulses were applied, the intensity very sharply increased from 100 s to 300 s. It might be due to the spontaneous conversion of initially formatted hydrophobic nano-pores into long-lived hydrophilic nano-pores. After 300 s, the intensity increased in each pulse application and saturated again, implying the reduction of concentration gradient of PI dye across the nano-pores. After 1200 s, the intensity became almost constant due to no PI dye uptake inside the single cell. However, there were no such results for 50 ns and 80 ns pulses, suggesting that these pulses were unable to create stable hydrophilic nano-pores from hydrophobic nano-pores on the cell membrane. Finally, in this LSCNEP design, 100 ns pulse was supposed to create the minimum number of membrane opening nano-pores for PI dye uptake. As a result for 100 ns pulses, the delivery efficiency was low (60%), although the cell viability was very high (94%). For ns pulse duration, the viability increased possibly because of very fast membrane resealing due to lower opening nano-pore and smaller affected membrane areas. Fig. 4(b), (d) and (f) shows the intensity distribution at different durations for 15 ms, 500 μs and 100 ns pulses. From this intensity profile, it was also clear that the intensities increased with the increasing time.

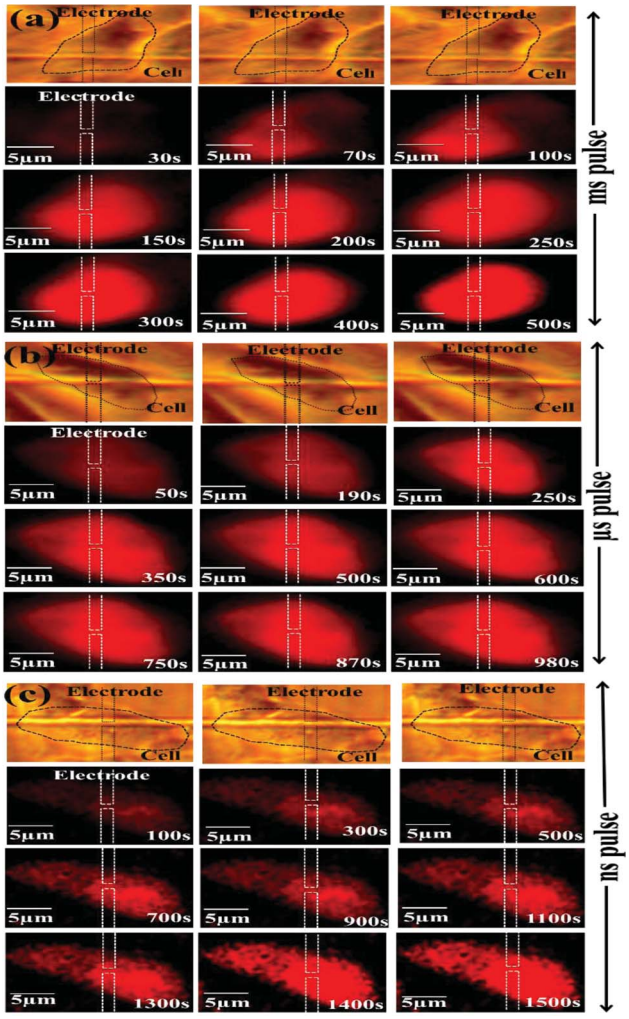

Fig. 3 Fluorescent microscopic images of HeLa cells in various time scales with different pulse durations (including saturation mode at higher times): (a) fluorescent images for 6 Vpp 15 ms pulse at different time durations; (b) images for 6 Vpp 500 μs pulses at different time durations; (c) images for 6 Vpp 100 ns pulse at different time durations.

3.3.2 Quantum dots (QDs) and plasmid delivery. To analyze quantum dots and plasmid delivery, HeLa cells were initially incubated into the chip for 2 h before the experiment. When the cells were attached into the chip surface, $CdSxSe_{1-x}$/ZnS core nanocrystals coated with COOH, (Crystalplex, Pittsburgh, Pa., USA) functional ligands were introduced into the electroporation chamber and immediately 6 Vpp and 40 ms positive pulse (three pulses together) were applied for QD tracking into the single cell. Fig. 5(a)

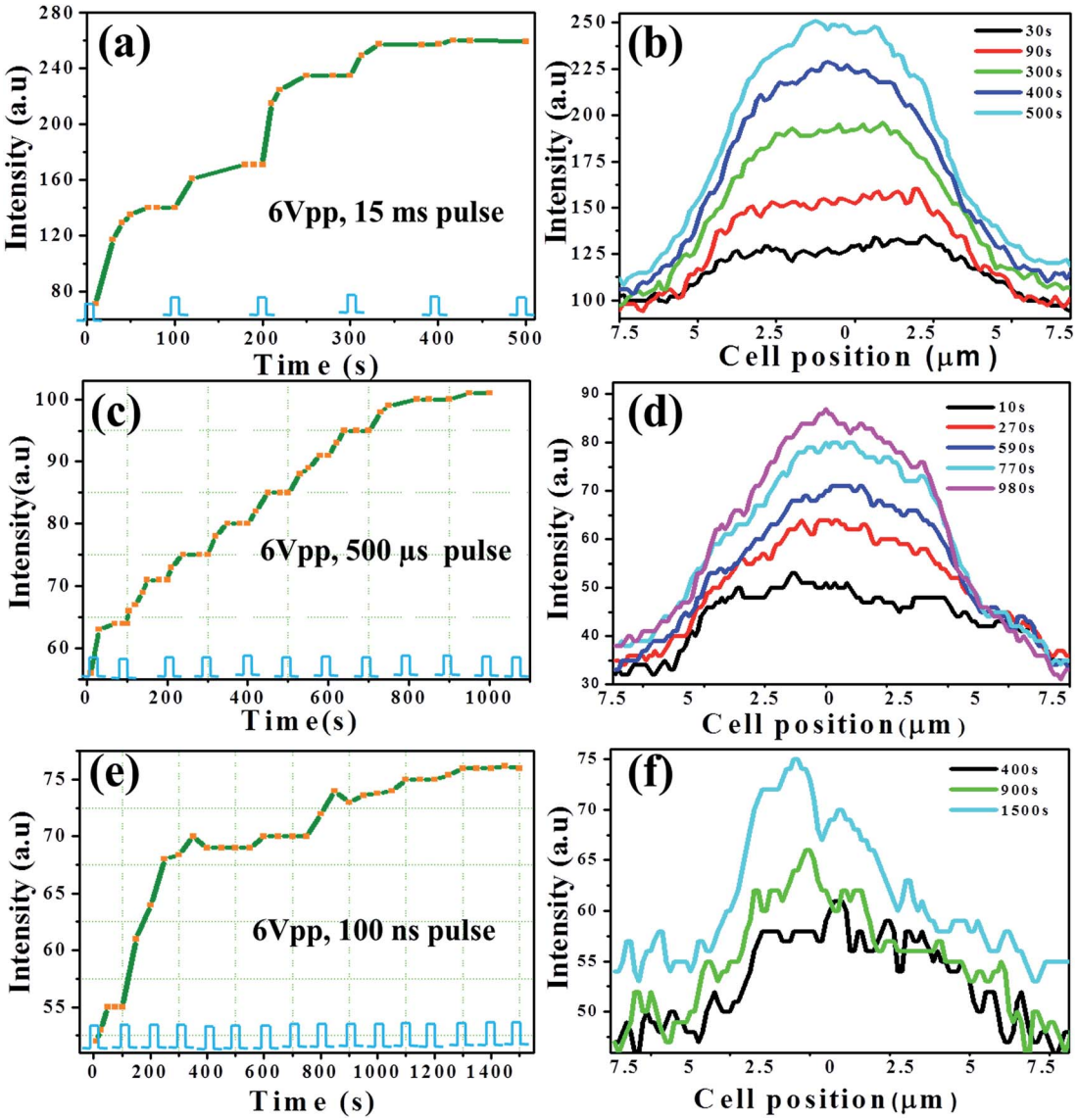

Fig. 4 Pore open-up and self-recovery processes with different intensity and different duration of pulses: (a) intensity profile after applying 6 Vpp 15 ms pulse (every single square wave positive pulse is applied every 100 s); (b) intensity variation with different cell position and different time for 15 ms pulse; (c) intensity profile for 6 Vpp 500 μs pulse (a single square wave positive pulse is applied every 100 s); (d) intensity variation with different cell position and different time for 500 μs pulse; (e) intensity profile for 6 Vpp 100 ns pulse (single square wave positive pulse is applied every 100 s); (f) intensity variation with different cell position and different time for 100 ns pulse.

demonstrates QD tracking inside the cell at different time scales. After 40 min, the intensity was almost constant, which indicated that QDs successfully entered inside the single cell. However, to introduce QDs into the cell, it took considerably longer time, compared to PI dye delivery because of a larger molecular weight, resulting in a lower diffusion rate of QDs. The size of each quantum dot was 5.5–6.5 nm, whereas the size of each PI dye was 0.69 nm in diameter and 1.55 nm in length (cylindrical approximation). Fig. 5(b) shows the vertical scanning of HeLa cells by confocal microscopy after the delivery of QDs. The step size of each scan was 1 μm. This scanning image was taken after 2 h of electroporation experiment. The scanning image shows that the HeLa cell appears to be semi-hemispherical with a diameter of approximately 12 μm to 15 μm. The delivery efficiency and cell viability of HeLa cell after QDs tracking were 75% and 80%, respectively.

For the plasmid experiment, we employed a 6 Vpp and 40 ms square wave positive pulse (three pulses together) on the cell to deliver pMax-E2F1 (Addgene, Cambridge, MA, USA) gene and visualized the protein expression inside the single cell. After pulse application and plasmid introduction, Hoechst 33342 (Invitrogen) and deep-red (C10046, Invitrogen) plasma membrane dye was employed for the nucleus and membrane staining of single cell.

The residual plasmids and staining solution were then washed out (after 10 min incubation) from the electroporation chamber, and the cell medium was added. The

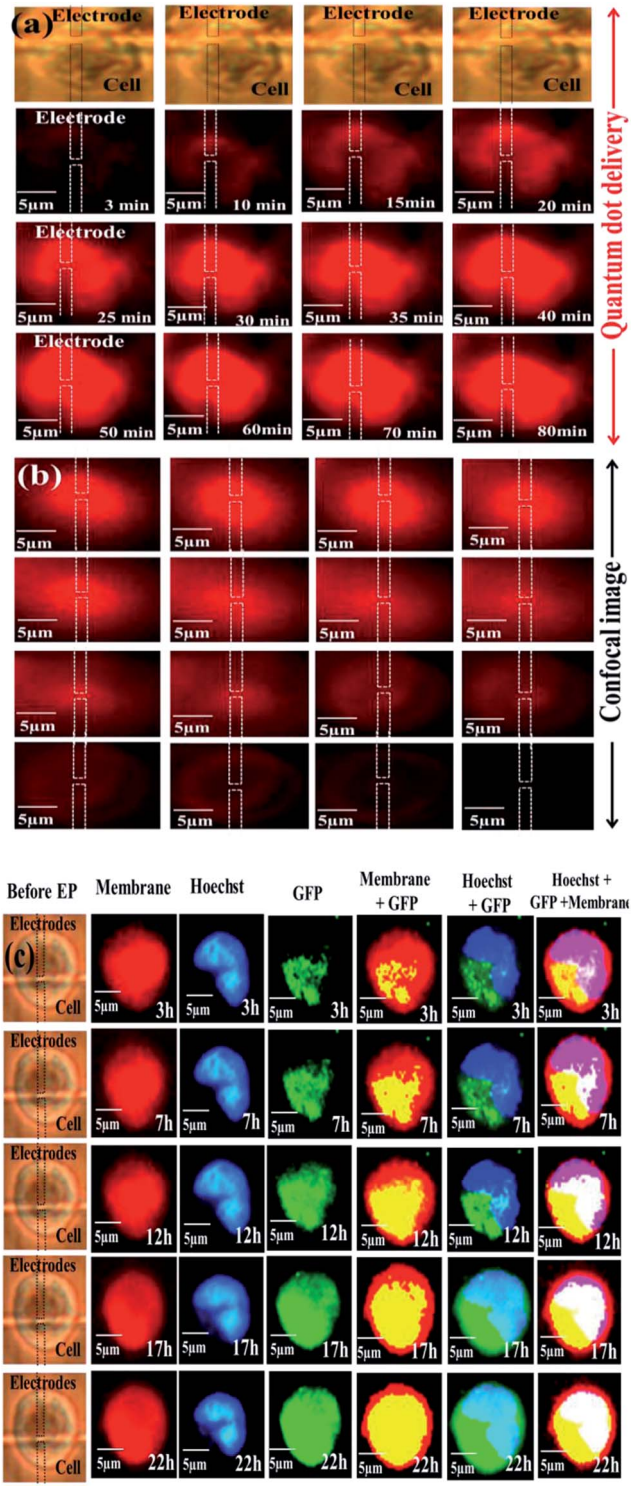

Fig. 5 Quantum Dots (QDs) and plasmid delivery inside single HeLa cells: (a) Quantum Dots delivery into HeLa cell with 6 Vpp 40 ms square wave positive pulse (three pulses) at different time durations; (b) Confocal microscopic images after QDs were delivered into single cell (step size = 1 μm); (c) Protein expression into single HeLa cell at 6 Vpp and 40 ms square wave positive pulse (three pulses). The cell membrane and nucleus were stained with Hoechst 33342 and deep-red plasma membrane dye.

LSCNEP chip was then incubated for 24 h for protein expression (we captured images at different intervals within 24 h). Fig. 5(C) shows the protein expression inside single HeLa cell with different time durations. In our experiment, after 15–22 h, protein were successfully expressed inside the single cell (see GFP column with 17 h and 22 h), and it took longer time because of a higher molecular weight (4.7×10^3 Da) when compared to PI dye (700 Da). After plasmid delivery, the transfection efficiency and cell viability were 70% and 85%. As per our knowledge, most of the literature either selected very high voltages (several volts to 1 kV) or longer time (one day to three days) to express QDs/plasmid delivery inside single cells.[9,32,49,50] However, in our LSCNEP system, it took less time (nearly 60 min for QDs and 15–22 h for plasmid) with a very low voltage (6 Vpp) requirement to deliver QDs/plasmid into single cell, suggesting a considerably effective method for generating long-lived hydrophilic pores by using the nano-electroporation method.

3.4 Delivery rate and cell viability

The delivery rate was calculated with PI dye delivery inside a single HeLa cell with different applied voltages (4 Vpp–7 Vpp) and different pulse durations (15 ms, 500 μs and 100 ns). However, to achieve efficient delivery rates with higher cell viability, we considered that 6 Vpp voltage was ideal for the nano-electroporation experiment. The viability was tested by using calcein AM and PI dye.

3.4.1 Millisecond, microsecond and nanosecond pulse effect. Fig. 6 shows the delivery rates and cell viability for 15 ms, 500 μs and 100 ns pulse, respectively, with different applied voltages. As observed in Fig. 6(a), the delivery rates for 15 ms pulses were as high as 90% for 6 Vpp applied voltage (black line). A high delivery rate was achieved due to higher voltage with higher TMP to easily reach cell membrane threshold values. For microsecond pulses, the molecular delivery rate was 80% for 6 Vpp applied voltage (red line). However, for a 100 ns pulse (green line), the delivery rate was very low, 60% for 6 Vpp applied voltage. The lower voltages (4 Vpp and 5 Vpp with 100 ns) were not enough to overcome the membrane threshold values.

The cell viability was tested using cell permeable calcein AM and cell impermeable PI dye. After electroporation experiment, PBS was washed away and DMEM medium was immediately introduced into the chamber, and it was then incubated. After 1 h, the medium was washed away and dyes were introduced (calcein AM and PI dye) with PBS for cell imaging. For 15 ms pulse, the cell viability was 80% for 6 Vpp applied voltage; however, for 500 μs pulse, 90% viability was achieved for 6 Vpp external voltages. For nanosecond pulses, the viability of the HeLa cell was as high as 94%, which may be due to a very small affected membrane area and a less toxic effect during the electroporation process. Fig 6(b)–(d) shows the cell viability using calcein AM and PI dye for 15 ms, 500 μs and 100 ns pulse, where the maximum cells are viable after the electroporation experiment (green colour).

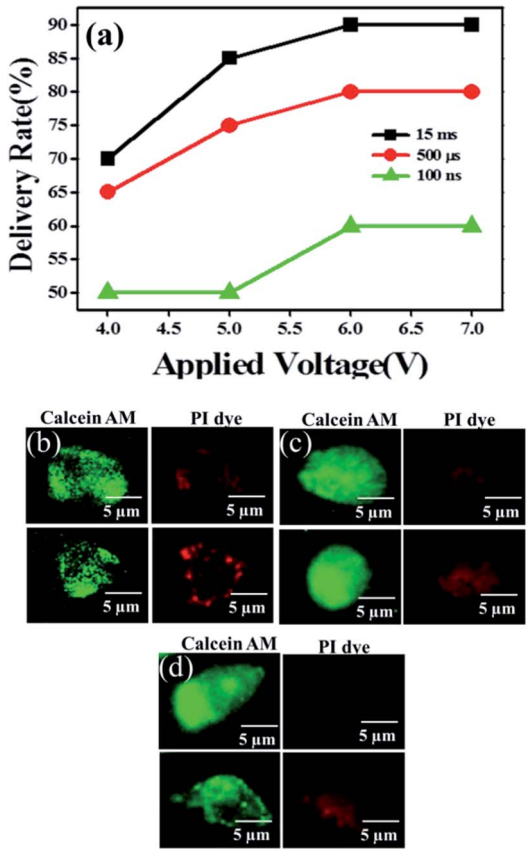

Fig. 6 Delivery rate and cell viability: (a) delivery rate for 15 ms (black line), 500 μs (red line) and 100 ns (green line) single square wave positive pulses with different applied voltages (4 Vpp–7 Vpp); (b) cell viability for 15 ms pulse with 6 Vpp applied voltage; (c) cell viability for 500 μs pulse with 6 Vpp applied voltage: (d) cell viability for 100 ns pulse with 6 Vpp applied voltage.

4. Conclusions

We have demonstrated a well-controlled, sequential, localized single cell nano-electroporation with membrane reversibility using an intense electrical field with different pulse durations. The SiO_2 layer not only performed key roles in reducing harmful reactions between the two nano-electrodes, but it also reduced the resistive heating effect on the membrane surface resulting in the reduction of cell toxicity. Lower voltage with a single square wave positive pulse can easily deliver molecules inside the single cell, whereas a higher number and duration of pulses can deliver ODs/plasmids inside the cytosol with higher transfection efficiency and cell viability. For ultra-short nanosecond pulses, the maximum cell viability was observed due to less affected membrane area; however, the minimum molecular delivery rate was observed when compared to millisecond and microsecond pulses. In the context of other studies, our experiment delivered QDs/plasmid faster with lower applied voltage into a single cell using the LSCNEP technique.

Acknowledgements

The authors greatly appreciate the financial support from National Science Council (NSC) of Taiwan ROC through National Nanotechnology and Nanoscience Program under Contract no. NSC 101-2221-E-007-032-MY3, 102-2321-B-007-006, and 103-2321-B-007-004.

References

1 L. H. Yin and S. Q. Fu, *Stem Cells*, 1998, **16**(247), S2.
2 S. C. Wu, G. Y. L. Huang and J. H. Liu, *Biotechnol. Prog.*, 2002, **18**, 617.
3 R. M. Schmid, H. Weidenbach, G. F. Draenert, S. Liptay, H. Lührs and G. Adler, *Gut*, 1997, **41**, 549.
4 J. A. O'Brien and S. C. R. Lummis, *Nat. Protoc.*, 2006, **1**, 977.
5 D. H. Fuller, P. Loudon and C. Schmaljohm, *Methods*, 2006, **40**, 86.
6 S. Ohta, K. Suzuki, Y. Ogino, S. Miyagawa, A. Murashima and D. Matsumaru, *Dev., Growth Differ.*, 2008, **50**(6), 517.
7 K. K. Ewert, A. Ahmad, N. F. Bouxsein, H. M. Evans and C. R. Safinya, *Methods Mol. Biol.*, 2008, **433**, 159.
8 E. Neumann, M. Schaefer-Ridder, Y. Wang and P. H. Hofschneider, *EMBO J.*, 1982, **1**(7), 841.
9 P. E. Boukany, A. Morss, W.-C. Liao, B. Henslee, H. C. Jung, X. Zhang, B. Yu, X. Wang, Y. Wu, L. Li, K. Gao, X. Hu, X. Zhao, O. Hemminger, W. Lu, G. P. Lafyatis and L. J. Le, *Nat. Nanotechnol.*, 2011, **6**, 747.
10 S.-C. Chen, T. S. Santra, C.-J. Chang, T.-J. Chen, P.-C. Wang and F.-G. Tseng, *Biomed. Microdevices*, 2012, **14**(5), 811.
11 T. S. Santra and F.-G. Tseng, *Micromachines*, 2013, **4**, 333–356.
12 R. Crystal, *Science*, 1995, **270**, 404.
13 S. C. Hartman, D. M. Appledorn and A. Amalfitano, *Virus Res.*, 2008, **132**(1–2), 1.
14 D. Luo and W. M. Saltzman, *Nat. Biotechnol.*, 2000, **18**, 33.
15 G. L. Prasanna and T. Panda, *Bioprocess Eng.*, 1997, **16**, 261.
16 K. Kim, J. A. Kim, S.-G. Lee and W. G. Lee, *Nanoscale*, 2012, **4**, 5051.
17 A. Valero, F. Merino, F. Wolbers, R. E. Luttge, L. Vermes, H. Andersson and A. van den Berg, *Lab Chip*, 2005, **5**, 49.
18 J. A. Kim, K. Cho, M. S. Shin, W. G. Lee, N. Jung, C. Chung and J. K. Chang, *Biosens. Bioelectron.*, 2008, **23**, 1353.
19 J. C. Weaver, *Electroporation Theory*, Humana Press, Totowa, New Jersey, 1995, p. 1.
20 K. A. DeBruin and W. Krassowska, *Biophys. J.*, 1999, **77**, 1213.
21 K. A. DeBruin and W. Krassowska, *Biophys. J.*, 1999, **77**(3), 1225.
22 S. Movahed and D. Li, *Microfluid. Nanofluid.*, 2011, **10**, 703.
23 Y. C. Lin and M. Y. Huang, *J. Micromech. Microeng.*, 2001, **11**(5), 542.
24 Y. Huang and B. Rubinsky, *Sens. Actuators, A*, 2003, **104**(3), 205.
25 J. E. Bestman, R. C. Ewald, S. L. Chiu and H. T. Cline, *Nat. Protoc.*, 2006, **1**(3), 1267.
26 A. Agarwal, I. Zudans, E. A. Weber, J. Olofsson, O. Orwar and G. S. Weber, *Anal. Chem.*, 2007, **79**(10), 3589.

27 D. Nawarathna, K. Unal and H. K. Wickramasinghe, *Appl. Phys. Lett.*, 2008, **93**, 153111.
28 M. B. Fox, D. C. Esveld, A. Valero, R. Luttge, H. C. Mastwijk, P. V. Bartels, A. van den Berg and R. M. Boom, *Anal. Bioanal. Chem.*, 2006, **385**, 474.
29 J. Wang, M. J. Stine and C. Lu, *Anal. Chem.*, 2007, **79**, 9584.
30 J. A. Lundqvist, F. Sahlin, M. A. Aberg, A. Strimberg, P. S. Eriksson and O. Orwar, *Proc. Natl. Acad. Sci. U. S. A.*, 1998, **95**, 10356.
31 J. Olofsson, M. Levin, A. Stromberg, S. G. Weber, F. Ryttsen and O. Orwar, *Anal. Chem.*, 2007, **79**, 4410.
32 X. Xie, A. M. Xu, S. Leal-Ortiz, Y. Cao, C. C. Garner and N. A. Melosh, *ACS Nano*, 2013, 7(5), 4351.
33 W. Kang, F. Yavari, M. Minary-Jolandan, J. P. Giraldo-Vela, A. Safi, R. L. McNaughton, V. Parpoli and H. D. Espinosa, *Nano Lett.*, 2013, **13**, 2448.
34 N. Jakilaakso, E. Salm, A. Chen, L. Millet, C. D. Guevara, B. Dorvel, B. Reddy Jr, A. E. Karlstrom, Y. Chen, H. Ji, Y. Chen, R. Sooryakumar and R. Bashir, *Lab Chip*, 2013, **13**, 336.
35 T. S. Santra, H.-Y. Chang, P.-C. Wang and F.-G. Tseng, *Appl. Phys. Lett.*, 2013, **103**, 233701.
36 Y. Hoshiy and R. Ohki, *Electrochim. Acta*, 1999, **44**, 3927.
37 M. Hibino, H. Itoh and K. Kinosita Jr, *Biophys. J.*, 1993, **64**, 1789.
38 K. Kinosita and T. Y. Tsong, *Nature*, 1997, **268**, 438.
39 H.-Y. Wang, A. K. Bhunia and C. Lu, *Biosens. Bioelectron.*, 2006, **22**, 582.
40 J. C. Weaver and Y. A. Chizmadzhev, *Bioelectrochem. Bioenerg*, 1996, **41**, 135.
41 X.-M. Xu, M.-H. Yoo, B. A. Carlson, V. N. Gladyshev and D. L. Hatfield, *Nat. Protoc.*, 2009, **4**, 1338.
42 X. W. Dong, S. Goregoaker, H. Engler, X. Zhou, L. Mark, J. Crona, R. Terry, J. Hunter and T. Pristley, *Neurosciences*, 2007, **146**, 812.
43 Y. Jiang and D. Price, *Cell Cycle*, 2004, **3**, 1151.
44 H. Yun and S. C. Hur, *Lab Chip*, 2013, **13**, 2764.
45 Z. L. Xie, S. L. Shao, J. W. Lv, C. H. Wang, C. Z. Yuan, W. W. Zhang and X. J. Xu, *Cell Biol. Int.*, 2011, **35**, 187.
46 B. Gabriel and J. Teissie, *Biophys. J.*, 1997, **73**, 2630.
47 J. A. Lundqvist, F. Sahlin, M. A. Aberg, A. Strimberg, P. S. Eriksson and O. Orwar, *Proc. Natl. Acad. Sci. U. S. A.*, 1998, **95**, 10356.
48 X. Zhao, M. Zhang and R. Yang, *Comm. Nonlinear. Sci. Numer. Simulat.*, 2010, **15**(5), 1400.
49 J. S. Yoo, N. Won, H. B. Kim, J. Bang, S. Kim, S. Ahn and K.-S. Soh, *J. Appl. Phys.*, 2010, **107**, 124702.
50 Y. Liu, M. Zhou, D. Luo, L. Wang, Y. Hong, Y. Yang and Y. Sha, *Biochem. Biophys. Res. Commun.*, 2012, **425**, 769.